Published in final edited form as:
J Biomed Nanotechnol. 2009 April ; 5(2): 182.

Size-Uniform 200 nm Particles: Fabrication and Application to Magnetofection

Lamar Mair[1], **Kris Ford**[2], **Rowshon Alam, Md.**[3], **Ryszard Kole**[3], **Michael Fisher**[3], and **Richard Superfine**[1,4,5,*]

[1]Curriculum in Applied Sciences and Engineering, University of North Carolina at Chapel Hill, Chapel Hill, North Carolina 27599, USA

[2]Department of Biomedical Engineering, University of North Carolina at Chapel Hill, Chapel Hill, North Carolina 27599, USA

[3]Department of Pharmacology, University of North Carolina at Chapel Hill, Chapel Hill, North Carolina 27599, USA

[4]Department of Physics and Astronomy, University of North Carolina at Chapel Hill, Chapel Hill, North Carolina 27599, USA

[5]Department of Computer Science, University of North Carolina at Chapel Hill, Chapel Hill, North Carolina 27599, USA

Abstract

We report on the fabrication of arrays of mono- and multimetallic particles via metal evaporation onto lithographically patterned posts, as well as the magnetic force calibration and successful magnetofection of iron particles grown via this method. This work represents the first instance in which metal evaporation onto post structures was used for the formation of released, shape-defined metal particles. Also, our work represents the first use of lithographically defined particles as agents of magnetofection. Using these techniques it is possible to create particles with complex shapes and lateral dimensions as small as 40 nm. Our demonstrated compositionally flexible particles are highly size-uniform due to their photolithographically defined growth substrates, with particle dimensions along two axes fixed at 200 nm; the third axis dimension can be varied from 20 nm to 300 nm during the deposition procedure. Atomic percent of metals incorporated into the particle volume is highly tunable and particles have been synthesized with as many as four different metals. We performed magnetic force calibrations on a single particle size for iron particles using an axially magnetized NeFeB permanent magnet and comparisons are made with commercially available magnetic beads. In order to evalutate their usefulness as magnetofection agents, an antisense oligonucleotide (ODN) designed to correct the aberrant splicing of enhanced green fluorescent protein mRNA, was successfully transfected into a modified HeLa cell line. Magnetically enhanced gene delivery was accomplished *in vitro* using antisense ODN-laden iron particles followed by application of a field gradient. Magnetically enhanced transfection resulted in a 76% and 139% increase in fluorescence intensity when compared to Lipofectamine and antisense ODN-loaded particles delivered without magnetic treatment, respectively. To our knowledge, these experiments constitute the first use of lithographically defined particles as successful agents for magnetically enhanced transfection of an antisense oligonucleotide.

*Author to whom correspondence should be addressed.

1. INTRODUCTION

Magnetic micro- and nanoparticles with a wide array of chemical and physical properties have been synthesized, characterized, modified, and utilized in materials science, biology and biochemistry.[1, 2] These particles have undergone particularly intense research due to their ability to interact chemically and biologically with a sample while providing the experimenter with a physical means by which to spatially manipulate the particle and its bound payload.[3] Attaching therapeutic agents,[4] DNA,[5] or antisense oligonucleotides[6] to magnetic particles for drug delivery applications has proven successful in an array of cell lines. Specifically, researchers have been effective in utilizing magnetic field gradients to increase the interaction probability and, consequently, the transfection efficacy, of various moieties attached to magnetic particles.

Although techniques have been developed to fabricate particles in the size range of 40 nm and below, there is a dearth of strategies for size uniform particles in the range of 20 nm to 1 micron. We present a technique that is capable of defining the lateral shape of the particle down to the resolution of lithography (~20 nm for electron beam lithography) while precisely controlling the particle composition and structure through sequential deposition of user selected metals or dielectrics.

Previous magnetofection experiments have been performed almost exclusively with commercially available colloidal polymer-iron oxide particles created via wet chemistry techniques.[6] Particles grown using photolithographic ally defined templates have been successfully transfected into cells,[7] however more effective delivery of an antisense ODN using these types of particles in conjunction with magnetofection protocols has not yet been reported. The ability to incorporate a variety of metals into a single particle and modulate each metal's concentration allows user-specific tunability on a single wafer platform, thereby expanding the metallic particle toolbox. Utilizing the various properties of metals also makes possible particles with an array of designed surface chemistries. For example, Fe_3O_4@Ag particles were recently developed, used as antimicrobial agents, and magnetically reclaimed from water samples;[8] Park et al. were successful in tuning the catalytic oxidation of CO by changing the composition ratios of Rh–Pt nanoparticles.[9] Also, FePt particles were synthesized and functionalized so as to produce photoswitchable ferromagnetic nanoparticles capable of operating at room temperature.[10] Optically controlling a particle's magnetic properties is an important step in realizing high density optical memory.[10]

Magnetofection aims to increase transfection rate by bringing the relevant gene in rapid and direct contact with a cell membrane, as well as decrease the amount of vector necessary for a single assay. While this is advantageous for *in vitro* experiments, the tool's major potential lies in remote controlled vector targeting *in vivo*.[11] Physical vapor deposition into ordered arrays of holes or onto posts has been performed using interferometric lithography for use in memory storage applications[12, 13] and the magnetic properties of these arrays have been studied.[14] More recently, lithographically defined templates have been used to create polymeric particles with exquisite control over particle shape and composition.[15–18] These methods are excellent examples of how patterned substrates offer flexibility in shape and composition which is difficult to produce using strictly chemical methods. However, they differ from our procedure in that they do not rely on metal evaporation onto a surface followed by particle harvesting. We demonstrate the ability to create versatile, size uniform metal particles incorporating from one to four metals in a single particle. We quantified the low-field particle susceptibility and the forces generated on these fabricated particles and compared them with commercially available particles. We demonstrate the usefulness of Fe particles made in this manner by the successful magnetofection of iron/iron oxide particles into HeLa EGFP-654 cells. The transfection successfully delivers antisense oligonucleotide, blocking a mutated, aberrant

splice site contained in the EGFP pre-mRNA, resulting in expression of the green fluorescent protein.

2. EXPERIMENTAL DETAILS

2.1. Lithographically Defined Photoresist Structures for Particle Fabrication

Standard photolithography techniques are used to produce 0.20 μm cylindrical posts 0.33 μm tall with 0.70 μm pitch. Briefly, Si wafers (6″) are RCA-cleaned in preparation for photolithography and an ASML 5500/950B Step and Scan photolithography tool (Triangle National Lithography Center, Raleigh, North Carolina) is used to produce post structures. A bottom antireflective coating (BARC) is applied to the wafer prior to photoresist deposition to prevent interfering reflectance from the wafer surface. Following exposure, development and liftoff a metal film is resistively evaporated onto the patterned wafer surface. The resulting film is a laterally conformal layer of metal over the entire wafer surface, leaving only the sidewalls of the vertical post structures exposed to solvents. Iron, iron–gold, nickel–gold–palladium, and nickel–gold–palladium–cobalt particles were created using this method. After metallization, templates were placed in acetone for 24 h, followed by sonication in acetone for 1 h, resulting in the dissolution of photoresist posts and release of evaporated particles (hereafter referred to as Post-Particles).The lateral particle size dimensions were closely defined by the patterned substrate. As shown in Figure 1, the patterned substrate resulted in posts with hemispherical tops. The hemispherical top surfaces of these posts resulted in particles which crescent shaped cross-sections. Figure 2(d) indicates this cross-sectional aspect of the particle shape. Uniformity in lateral dimension is exhibited by the TEM images in Figure 3 in which particles are viewed top-down.

2.2. Force Calibration

To understand the applicability of our particles for magnetofection, we calibrate the force generated on Fe particles created using this technique by an applied magnetic field gradient through the application of Stokes law. Specifically, magnetic fields due to permanent magnets or magnet arrays will play a role in future drug delivery applications of magnetic carriers.[19–22] Particle motion through water was characterized by applying a known field gradient (using a NdFeB permanent magnet) to particles in a closed sample well (20 μl).In the low field limit, the magnetic force on a particle is

$$F=\frac{\pi d^3}{4\mu_0}\left\{\frac{\mu_r-1}{\mu_r+2}\right\}\nabla(B^2) \quad (1)$$

where d is the bead diameter, μ_0 is the relative permeability of free space (in SI units), and μ_r is the relative permeability of the bead. A particle's permeability is related to its susceptibility via

$$\mu_r=\mu_0(1+\chi_v) \quad (2)$$

If force, particle diameter, and magnetic field (B) are known, then μ_r can be determined using Eq. (1). Susceptibility can then be calculated using Eq. (2).

The magnetic field and field gradient were measured to be sufficiently uniform over the 60 μm field of view.[23] Obtaining the solution viscosity (η), bead radius (a_b), and the bead velocity (v) allows us to use Stokes formula,

$$F=6\pi\eta a_{\mathrm{b}}v \quad (3)$$

to calculate the average force on each particle. Velocity measurements were also taken on Micromod nanomag® - D PEG-COOH 250 nm particles (Micromod Partikel-technologie GmbH) and Dynabeads® MyOne™ 1 μm iron oxide impregnated beads (Invitrogen) for comparison. The magnetic field was measured in 250 μm increments along the axis of the magnet; measurements were taken between 18 and 80 mm from the magnet face. A 100× objective was used to image particles (in an epi-illumation configuration) and video was collected at 20 frames per second using a Pulnix PTM-6710CL camera. Video tracking and analysis software[24] was used to calculate particle velocities under a given field gradient.

2.3. Attachment of Antisense Oligonucleotide to Fe Particles

Particles may be functionalized while still attached to their posts or after release from the wafer. Polyethyleneimine is commonly used to bind DNA to particles11, 25–28 and is used here to electrostatically interact with a EGFP-correcting oligodeoxyribonucleic acid (ODN).Resina et al. have delivered splice-switching oligonucleotides to HeLa pLuc cells for the successful modulation of a transgene.29 These antisense ODN constructs were synthesized using phosphoramidite chemistry (courtesy of Md. Rowshon Alam, University of North Carolina at Chapel Hill, Department of Pharmacology).30 Specifically, the oligomer consists of 20 nucleotides (5′-GTT ATT CTT TAG AAT GGT GC-3′) and is antisense to the cryptic splice site activated on intron 2 of the IVS2-654 mutant beta-globin gene in the HeLa EGFP-654 cells. The ODN is modified with a 2′-O-methyl and phosphorothioate internucleotide backbone, resulting in increased stability and protection against degradation by nucleases.

PEI was bound to the Fe Post-Particles by mixing the particles (1 mg/ml) with 0.1 mg PEI for 4 h in a DI water adjusted to pH 10 using 0.1 M NaOH. At this pH the zeta potential of the particles is sufficiently low to electrostatically bind cationic PEI to the particle surface. To bind the oligonucleotides, PEI-labeled particles (1 mg/mL) were mixed with oligonucleotide (50 μM) at a 5:1 ratio by volume with an equal part of phosphate buffered saline. This mixture was allowed to rotate for 1 hour at room temperature. For Lipofectamine transfection experiments, antisense oligonucleotide was complexed with Lipofectamine 2000 at a 1:1 volume ratio (Invitrogen, Carlsbad, CA).Lipofectamine 2000 is a common transfection agent used for introducing genes into cells, both transiently and stably.

2.4. Cell Culture and Magnetofection Experiments

The HeLa cell line EGFP-654 expresses a construct in which the coding region of the of enhanced green fluorescent protein (EGFP) is interrupted by the mutated beta-globin intron. The cell line is grown at 36.5 °C and 3.5% CO_2 in Dulbecco's Modified Eagle Medium with F-12 nutrient mixture (Invitrogen, Carlsbad, CA) with L-glutamine and HEPES buffer supplemented with 10% fetal bovine serum. Growth media was further supplemented with 10% antibiotic-antimycotic (Penicillin-Streptomyocin and Amphotericin B, Invtitrogen).

HeLa EGFP-654 cells were plated at 5000 cells per well 24 hours before transfection in a Nunc 384 well plate. Before transfection cell media was replaced with Opti-MEM I Reduced-Serum Medium (Invitrogen, Carlsbad, CA).The cells were treated for 1 hour with a 200 nM dose of antisense ODN complexed with 200 nm Fe nanoparticles with and without a permanent magnetic field. Control experiments were performed using untreated and Lipofectamine treated (no particles) HeLa EGFP-654 cells in order to compare the efficacy of gene transfection using these particles. Also, in order to assess the differences between free-floating PEI-ODN complex and particle and Lipofectamine transfections, PEI (50% w/w, 60,000 *MW*) was diluted 1:5000

and conjugated with the antisense oligonucleotide. It was also added to the cell culture at 200 nM and allowed to incubate for 1 hour, at which time the media was replaced with fresh media.

For magnetic nanoparticle transfections one sample was placed over the NdFeB magnets for 1 hour and a second sample did not receive an external magnetic field. The media was changed in all samples to D-MEM F-12 with 10% FBS after 1 hour. Replacing media after the field application removed free-floating ODN-laden particles from the solution, as well as any free ODN which may have separated from particles, thus eliminating the possibility for transfection later in the experiment. The cells were incubated for an additional 23 hours before imaging. The total duration of the experiment was 24 hours. After 24 hours fluorescence microscopy was used to quantify the transfection efficacy. Treated and untreated cells were imaged using a Nikon Eclipse TE 2000-E inverted optical microscope (Tokyo, Japan) with a 40× objective. Images were taken using a Photometrics Cascade II 512 electron multiplying CCD digital camera (Roper Scientific, Inc., Tuscon, AZ) and background fluorescence was established by performing segmentation imaging on highest intensity cells in untreated samples. Cells measuring above this background fluorescence in treated samples were measured for mean intensity using segmentation. Mean background fluorescence was subtracted to determine the true mean intensities above background for treated cells. An average of 20 images were taken of each well and weighted mean intensities were summed over all images.

3. RESULTS AND DISCUSSION

3.1. Compositionally Diverse Particles

Using these templates particles with varying compositions have been made, including Fe, Fe–Au, Ni–Au–Pd, and Ni–Au–Co–Pd particles. Energy-dispersive X-ray spectroscopy (EDS) analysis was performed on five particle compositions using a Hitachi S-4700 FE-SEM. Three of these particles were Fe–Au particles with varying metal ratios (particles a–c in Fig. 4), one was a Au–Ni–Pd particle (particle d in Fig. 4), and the other was a Au–Co– Ni–Pd particle (particle e in Fig. 4).For compositional analysis, all sample substrates were immersed in acetone (using a 20 ml scintillation vial) for 24 h and sonicated for 1 h, after which the growth substrates were removed from the scintillation vial and the particles were rinsed three times using magnetic separation. Subsequently, particles were deposited from acetone onto Ted Pella carbon sample substrates, concentrated under a magnetic field gradient, and imaged immediately after drying. EDS data was collected at 13 kV accelerating voltage and 20 μA beam current. Figure 4 indicates the five spectra that were collected along with the atomic compositions of each particle batch created.

3.2. Force Calibration of Fe Post-Particles

We determined the forces on 1 μm superparamagnetic Dynabeads® MyOne™, 250 nm superparamagnetic Micromod nanomag® particles, and 200 nm Fe Post-Particles. MyOne™ and Micromod particles were each diluted 1/10000 v/v prior to beginning force experiments. Sample volumes were placed in a closed well to eliminate the effects of evaporation and sample drift; the well was spaced a calibrated distance from the face of a permanent magnet. We delivered 20 ul of diluted particle solution (25 °C) into the well and observed particle velocities. We identified many-particle aggregates and aligned strings of particles and omitted them from the tracking results. Due to their shape-uniformity, aggregates or aligned strings of two or more MyOne™ beads were clearly evidenced by their lemniscate-shaped image and multi-particle strings were not tracked. The shape heterogeneity of Micromod 250 nm particles makes single particle identification more difficult. MyOne™ beads did not aggregate, while approximately 30% of objects in Post-Particle samples appeared to be incorporated into field-aligned particle chains and 50% of objects in Micromod nanomag® samples were considered aggregates. Although both Micromod and Post-Particles exhibited connected multi-particle groupings

during the experiment, these groupings displayed drastically different morphological characteristics within each sample. Micromod particles were observed as both spheres of varying diameter and as field-aligned chains of particles. While aligned strings of Post-Particle were observed, spherically shaped agglomerates of varying diameter were not seen. A reticule was used to determine that the pixel dimension of the video data taken was 124 nm^2. Particle velocities were established using in-house particle tracking software.[24] Tracked particles were chosen based on dimensions of the particle image. Low-number collections (1–3 particles) of Micromod and Post-Particles were not guaranteed exclusion from the tracked data due to their size being close to the optical resolution limit of our microscope. Figure 5 shows the displacement versus time data for the three particles tested.

From the observed particle velocities we calculated the applied forces on the particles due to the magnetic field gradient via Stokes formula. We tracked 45 beads for each type of particle, all tracks occurring in the same magnetic field gradient. Average velocities were 11.1 μm/s, 5.9 μm/s, and 10.7 μm/s for Dynabeads® MyOne™, Micromod 250 nm, and 200 nm Fe Post-Particles, respectively; the resulting average forces applied to these beads were 138 ± 22 fN, 18 ± 2 fN, and 26 ± 5 fN for Dynabeads® MyOne™, Micromod 250 nm, and 200 nm Fe Post-Particles, respectively. Although we have treated the resulting force histogram shown in Figure 6 as monomodal for all particle types, the shape of the Post-Particle distribution suggests a bimodal force distribution for Fe Post-Particles, the first mode existing at 22 fN and the second mode occurring at 30 fN. This indicates force data arising from two discrete populations, namely a single particle population and a double particle population. An aligned pair or triplet of particles is expected to experience more force in a given field and field gradient.

We use this force data to calculate susceptibility χ_v and magnetization M for each particle type. As noted earlier, the force on compositionally equivalent particles which vary in size is proportional to the cube of the particle diameter, $F \sim d^3$.The force applied to a particle in the low magnetic field limit depends on the particle volume (V), the difference in magnetic susceptibilities (Δ_χ) (between the particle susceptibility, $\chi_{particle}$, and the surrounding material's susceptibility, $\chi_{surround}$), and the field and field gradient of the magnetic field:

$$F = \left\{ \frac{V \cdot \Delta\chi}{2\mu_0} \right\} (B \cdot \nabla) B \tag{4}$$

Particles we tested varied by size and composition. MyOne™ beads consist of γ-Fe_2O_3 dispersed in a polystyrene matrix and coated with a thin polymer layer; Micromod particles consist of Fe_3O_4 dispersed in a silica-fortified polysaccharide matrix;[31] 200 nm Fe Post-Particles are iron particles with a native oxide at the particle surface. Using Eq. (4) and the calculated average forces applied to each type of particle we obtain the volumetric particle susceptibilities. Using the calculated χ_v and the known magnetic field of 0.081 T, as well as the relationships among B, M, and H [namely, $\chi_v = M/H$ and $B = \mu_0(M + H)$] we determine each particle's magnetization in the given 0.081 T field. These results are summarized in Table I. The calculated magnetization, M, for the particles is equal to the magnetic moment per unit volume, $M = m/V$. The magnetization value for Fe Post-Particles was only slightly higher than that of the Micromod particles, while the susceptibilities for Fe Post-Particles was 171% larger than that of Micromod particles.

We now compare our calculations for MyOne™ and Micromod particles with other reports. Previously, researchers have recorded various values for the magnetization and volumetric susceptibility of MyOne™ [32, 33] and Micromod[34, 35] particles. Our measurements of MyOne™ bead susceptibility agrees with these previous reports; our measurements of Micromod bead susceptibility is significantly higher than other reports. This strongly indicates that the

Micromod particles tracked and tabulated during our experiment were actually small packets of particles clumped together; our experiments yielding average per particle χ_v values of 200% and 260% of those previously reported[34, 35] indicates that these small packets typically consisted of two or three particles attached to one another.

Understanding the force-to-size ratio for magnetic particles in a known field and field gradient is crucial for informed estimates of particle translational performance. Importantly, this force-to-size ratio is highly dependent upon the specific material(s) incorporated into a particle. Most particles synthesized via wet chemical methods are composed of magnetite or maghemite.[1] As stated previously, for spherical particles of a given material in a given field, a 200 nm particle would be expected to experience 0.80% and 51% of the force experienced by a 1 μm and 250 nm particle, respectively. Deviations from this pattern must indicate geometric or compositional differences among the particles. Our 200 nm Post-Particles experienced a force 19% that exhibited by 1 μm Dynal beads and 144% that experienced by the Micromod particles, drastically larger than the expected 0.80% and 51%, respectively. Although geometric differences do exist among the particles tested, these differences are too small to cause such large disparities in particle force. These large discrepancies in force mean that our Post-Particles are made from a different material than either of the two commercially available particles. These commercial particles are composed of iron oxide grains smaller than the single domain size[31, 36] and, consequently, MyOne™ and Micromod beads are both superparamagnetic.[31, 36] Collected video data of the absence of remanence-induced aggregation confirmed this fact. In the absence of a magnetic field we observed that MyOne™–MyOne™ and Micromod-Micromod bead collisions did not result in permanent bead aggregation. This is expected for superparamagnetic particles. In the absence of a magnetic field superparamagnetic beads have no remnant magnetization and therefore no permanent dipole moments. Consequently, there were no dipole–dipole attractive forces between superparamagnetic particles to cause aggregation. In contrast, chain-like aggregation outside of a magnetic field was observed in our Post-Particles. Video data collected in the absence of an applied field showed non-reversible particle chaining (the agglomerates were not included in the force data), indicating that our Post-Particles were ferromagnetic. Ferromagnetic particles, once exposed to a magnetic field, exhibit a net magnetization which exists inside the volume despite the absence of an applied field. The fact that Post-Particles had comparatively large force-to-size ratios (relative to MyOne™ and Micromod particles) in the applied field is due to these differences in magnetic ordering. While MyOne™ and Micromod particles are composed of sub-20 nm grains of uniformly oxidized iron (γ-Fe_2O_3 and Fe_3O_4, respectively),[36, 37] our Post-Particle fabrication technique essentially creates arrays of size-uniform metallic clusters with grain sizes significantly larger than 20 nm. These grains are not uniformly oxidized and contain segments of pure Fe; this is not present in either of the superparamagnetic particles. This compositional difference explains the large discrepancy in actual and expected force-to-size ratios for our Post-Particles due to the fact that ferromagnetic materials have larger susceptibilities in a given field than do superparamagnetic materials. It should be noted that we have used the equation $\chi_v = M/H$ to calculate magnetization for all particles. This assumption does not hold precisely for ferromagnetic materials. The non-linear hysteresis loop of ferromagnetic materials makes this only an approximation. We expect this to be an underestimate as our experiments were performed in the low field range for ferromagnetic particles and because in low fields hysteresis curves for ferromagnetic materials typically exhibit steep slopes in small applied H fields.[38]

3.3. Magnetically Enhanced Cell Transfection

The general mechanism of the magnetic transfection starts with introducing the DNA-particle complexes into the cell media. A magnetic field is applied to direct the particles to the cell membrane. The particles come in contact with the cell membrane and are eventually taken into

the cytoplasm via endocytosis. The particle becomes encapsulated by a membrane-bound endosome as it is moved into the cellular interior. The PEI polymer has the capability to disrupt this membrane through a process called endosomolysis.[39] The PEI seems to elicit a substantial proton influx into the endosome ensued by a passive chloride influx. This causes osmotic swelling of the endosome, causing its rupture, and the subsequent release of the particle and genetic products. From here, a certain portion of the DNA is released from the particle to perform its designed function.

Although lithography techniques have gained popularity as a means of tailoring particle shape and composition,[15–17, 40] increased transfection via magnetofection using these types of particles has yet to be reported. In order to test the comparative efficacy of EGFP turn-on via particle delivery of ODN, five sets of cell treatments were established: untreated cells, cells dosed with only the PEI-ODN complex, cells dosed with antisense ODN-bound 200 nm Fe Post-Particles delivered without a magnetic field gradient, antisense ODN-bound 200 nm Fe Post-Particles delivered in the presence of a field gradient, and Lipofectamine 2000. Figure 7 shows representative images from each treatment course. The efficacy of magnetofection using our Post-Particles is clearly evidenced by the increased expression of EGFP. The increased fluorescence is a product of particles penetrating the cell membrane, delivering antisense ODNs to the cell nucleus, and aberrant splicing of EGFP pre-mRNA being corrected. Results from segmentation analysis of EGFP-expressing cells indicate a 76% increase in fluorescence intensity of ODN-loaded magnetic particles (with magnetic gradient applied) over Lipofectamine as well as a 139% increase in intensity over the non-magnetic control (Fig. 8). Also, as evidenced by images taken throughout the well, the rate of transfection was significantly higher in the magnetic sample over the non-magnetic control.

Magnetofection experiments exhibited only low levels of cell death (less than 5% overall) as observed through bright field microscopy and no evidence was seen that our particles increased cytotoxicity. However, our transfection times were 1 hour, and as such, possibly not a long enough time frame to accurately gauge toxicity levels. Toxicity experiments performed over extended periods would provide greater information regarding the comparative toxicity of our particles. Likewise, untreated HeLa EGFP-654 cells were unresponsive to the applied magnetic field and showed no visible signs of increased cytotoxicity during the experiment. It has been noted previously that an applied magnetic field enhances the transfection rate. The general mechanism by which this increased endocytosis is not clear.[41] It is accepted that the process of magnetofection decreases the time necessary for cell–particle interactions to occur by magnetically placing the ODN-laden particles spatially near or on the cell membrane. Researchers have explored the application of oscillating fields[41, 42] and have speculated that the oscillating field increases efficiency of endocytosis and may also cause endosomal release.

4. CONCLUSION

Multimetallic particles via physical vapor deposition onto lithographically defined substrates offers a method by which to produce highly size and shape uniform particles. Our technique allows user-specific metal compositions and concentrations, making this technique useful for tailoring the particle properties to a high degree. Particle velocities resulting from the application of a known magnetic field gradient were used to calculate the average force applied to particles and compare this with average forces applied to commercially available particles in the same field gradient. Particle susceptibilities were calculated and compared with expected values based on the particle composition. The significant forces applied to these nanoscale particles in the applied field gradient makes them excellent candidates for biophysical force experiments where small size is preferred, such as intracellular environments. Finally, results represent the first time lithographically-templated particles have been used in conjunction with magnetofection to deliver genes to cells.

Acknowledgments

The authors would like to thank Letian Lin for TEM imaging of Post-Particle samples, David Vellenga and Joan O'Sullivan for their contribution via the Triangle National Lithography Center, Raleigh, North Carolina, Professor Joseph DeSimone for graciously allowing us to use his reticle, the Chapel Hill Analytical and Nanofabrication Laboratory (CHANL, especially Carrie Donley and Wallace Ambrose) and E. Timothy O'Brien for help with cell cultures. We gratefully acknowledge financial support from the National Cancer Institute (the Carolina Center of Cancer Nanotechnology and Excellence, NIH-5-654-CA119373-02) and the National Institutes of Health (including Grant Nos. P41-EB002025-24A1 and R01-EB000761, and program project grant 5-PO1-GM059299).

References and Notes

1. Gupta AK, Gupta M. Synthesis and surface engineering of iron oxide nanoparticles for biomedical applications. Biomaterials 2005;26:3995. [PubMed: 15626447]
2. Pankhurst QA, Connolly J, Jones SK, Dobson J. Applications of magnetic nanoparticles in biomedicine. J. Phys. D: Appl. Phys 2003;36:R167.
3. Tanase M, Felton EJ, Gray DS, Hultgren A, Chen CS, Reich DH. Assembly of multicellular constructs and microarrays of cells using magnetic nanowires. Lab Chip 2005;5:598. [PubMed: 15915251]
4. Salem AK, Searson PC, Leong KW. Multifunctional nanorods for gene delivery. Nat. Mater 2003;2:668. [PubMed: 12970757]
5. Chorny M, Polyak B, Alferiev IS, Walsh K, Friedman G, Levy RJ. Magnetically driven plasmid dna delivery with biodegradable polymeric nanoparticles. FASEB J 2007;21:2510. [PubMed: 17403937]
6. Krotz F, de Wit C, Sohn HY, Zahler S, Gloe T, Pohl U, Plank C. Magnetofection-a highly efficient tool for antisense oligonucleotide delivery *in vitro* and *in vivo*. Mol. Ther 2003;7:700. [PubMed: 12718913]
7. Euliss LE, DuPont JA, Gratton S, DeSimone J. Imparting size, shape, and composition control of materials for nanomedicine. Chem. Soc. Rev 2006;35:1095. [PubMed: 17057838]
8. Gong P, Li HM, He XX, Wang KM, Hu JB, Tan WH, Zhang SC, Yang XH. Preparation and antibacterial activity of Fe_3O_4Ag nanoparticles. Nanotechnology 2007:18.
9. Park JY, Zhang Y, Grass M, Zhang T, Somorjai A. Tuning of catalytic co oxidation by changing composition of rh-pt bimetallic nanoparticles. Nano Lett 2008;8:673. [PubMed: 18225941]
10. Suda M, Nakagawa M, Iyoda T, Einaga Y. Reversible photo-switching of ferromagnetic fept nanoparticles at room temperature. J. Am. Chem. Soc 2007;129:5538. [PubMed: 17411039]
11. Plank C, Schillinger U, Scherer F, Bergemann C, Remy JS, Krotz F, Anton M, Lausier J, Rosenecker J. The magnetofection method: Using magnetic force to enhance gene delivery. Biol. Chem 2003;384:737. [PubMed: 12817470]
12. Farhoud M, Hwang M, Smith HI, Schattenburg ML, Bae JM, Youcef-Toumi K, Ross CA. Fabrication of large area nanostructured magnets by interferometric lithography. IEEE Trans. Magn 1998;34:1087.
13. Savas TA, Farhoud M, Smith HI, Hwang M, Ross CA. Properties of large-area nanomagnet arrays with 100 nm period made by interferometric lithography. J. Appl. Phys 1999;85:6160.
14. Ross CA, Haratani S, Castano FJ, Hao Y, Hwang M, Shima M, Cheng JY, Vogeli B, Farhoud M, Walsh M, Smith HI. Magnetic behavior of lithographically patterned particle arrays (invited). J. Appl. Phys 2002;91:6848.
15. Napier ME, Desimone JM. Nanoparticle drug delivery platform. Polym. Rev 2007;47:321.
16. Kelly JY, DeSimone JM. Shape-specific, monodisperse nanomolding of protein particles. J. Am. Chem. Soc 2008;130:5438. [PubMed: 18376832]
17. Hernandez CJ, Mason TG. Colloidal alphabet soup: Monodisperse dispersions of shape-designed lithoparticles. J. Phys. Chem. C 2007;111:4477.
18. Glangchai LC, Caldorera-Moore M, Shi L, Roy K. Nanoimprint lithography based fabrication of shape-specific, enzymatically-triggered smart nanoparticles. J. Controlled Release. 2007
19. Lubbe AS, Bergemann C, Brock J, McClure DG. Physiological aspects in magnetic drug-targeting. J. Magn. Magn. Mater 1999;194:149.
20. Alexiou C, Arnold W, Klein RJ, Parak FG, Hulin P, Bergemann C, Erhardt W, Wagenpfeil S, Lubbe AS. Cancer Res. 2000

21. Lubbe AS, Alexiou C, Bergemann C. Clinical applications of magnetic drug targeting. J. Surg. Res 2001;95:200. [PubMed: 11162046]
22. Alexiou C, Jurgons R, Seliger G, Iro H. Medical applications of magnetic nanoparticles. J. Nanosci. Nanotechnol 2006;6:2762. [PubMed: 17048480]
23. Fisher JK, Vicci L, Cribb J, O'Brien ET, Taylor RM, Superfine R. Magnetic force micromanipulation systems for the biological sciences. NANO 2006;1:191.
24. Taylor RM II. Video Spot Tracker 2008;8
25. Boussif O, Lezoualćh F, Zanta MA, Mergny MD, Scherman D, Demeneix B, Behr JP. A versatile vector for gene and oligonucleotide transfer into cells in culture and *in vivo*: Polyethylenimine. Proc. Natl. Acad. Sci. USA 1995;92:7297. [PubMed: 7638184]
26. Abdallah B, Sachs L, Demeneix BA. Non-viral gene transfer: Applications in developmental biology and gene therapy. Biol. Cell 1995;85:1. [PubMed: 8882514]
27. Gupta AK, Naregalkar RR, Vaidya VD, Gupta M. Recent advances on surface engineering of magnetic iron oxide nanoparticles and their biomedical applications. Nanomedicine 2007;2:23. [PubMed: 17716188]
28. Ragusa A, Garcia I, Penades S. Nanoparticles as nonviral gene delivery vectors. IEEE Trans. Nanobiosci 2007;6:319.
29. Resina S, Kole R, Travo A, Lebleu B, Thierry AR. Switching on transgene expression by correcting aberrant splicing using multi-targeting steric-blocking oligonucleotides. J. Gene Med 2007;9:498. [PubMed: 17471591]
30. Alam MR, Dixit V, Kang H, Li ZB, Chen X, Trejo JA, Fisher M, Juliano RL. Intracellular delivery of an anionic antisense oligonucleotide via receptor-mediated endocytosis. Nucleic Acids Res. 2008
31. Gruttner C, Teller J. New types of silica-fortified magnetic nanoparticles as tools for molecular biology applications. J. Magn. Magn. Mater 1999;194:8.
32. Lany M, Boero G, Popovic RS. Superparamagnetic microbead inductive detector. Rev. Sci. Instrum 2005;76:084301.
33. Fonnum G, Johansson C, Molteberg A, Morup S, Aksnes E. Characterisation of dynabeads® by magnetization measurements and mossbauer spectroscopy. J. Magn. Magn. Mater 2005;293:41.
34. Ejsing L, Hansen MF, Menon AK, Ferreira HA, Graham DL, Freitas PP. Planar hall effect sensor for magnetic micro-and nanobead detection. Appl. Phys. Lett 2004;84:4729.
35. Freitas, PP.; Ferreira, HA.; Cardoso, F.; Cardoso, S. A portrait of state-of-the-art research at the technical university of lisbon. Rozdzia/l Nanotechnology and the Detection of Biomolecular Recognition Using Magnetoresistive Transducers. Springer; 2007.
36. Amblard F, Yurke B, Pargellis A, Leibler S. A magnetic manipulator for studying local rheology and micromechanical properties of biological systems. Rev. Sci. Instrum 1996;67:818.
37. Gruttner C, Rudershausen S, Teller J. Improved properties of magnetic particles by combination of different polymer materials as particle matrix. J. Magn. Magn. Mater 2001;225:1.
38. Jiles, D. Introduction to Magnetism and Magnetic Materials. Chapman and Hall; 1991.
39. Huth S, Lausier J, Gersting SW, Rudolph C, Plank C, Welsch U, Rosenecker J. Insights into the mechanism of magnetofection using pei-based magnetofectins for gene transfer. Journal of Gene Medicine 2004;6:923. [PubMed: 15293351]
40. Rolland JP, Maynor BW, Euliss LE, Exner AE, Denison GM, DeSimone JM. Direct fabrication and harvesting of monodisperse, shape-specific nanobiomaterials. Curr. Opin. Colloid Interface Sci 2004;9:278.
41. McBain SC, Yiu HHP, El Haj A, Dobson J. Polyethyleneimine functionalized iron oxide nanoparticles as agents for dna delivery and transfection. J. Mater. Chem 2007;17:2561.
42. Kamau SW, Hassa PO, Steitz B, Petri-Fink A, Hofmann H, Hofmann-Amtenbrink M, Von Rechenberg B, Hottiger MO. Enhancement of the efficiency of non-viral gene delivery by application of pulsed magnetic field. Nucleic Acids Research 2006;34:e40. [PubMed: 16540591]

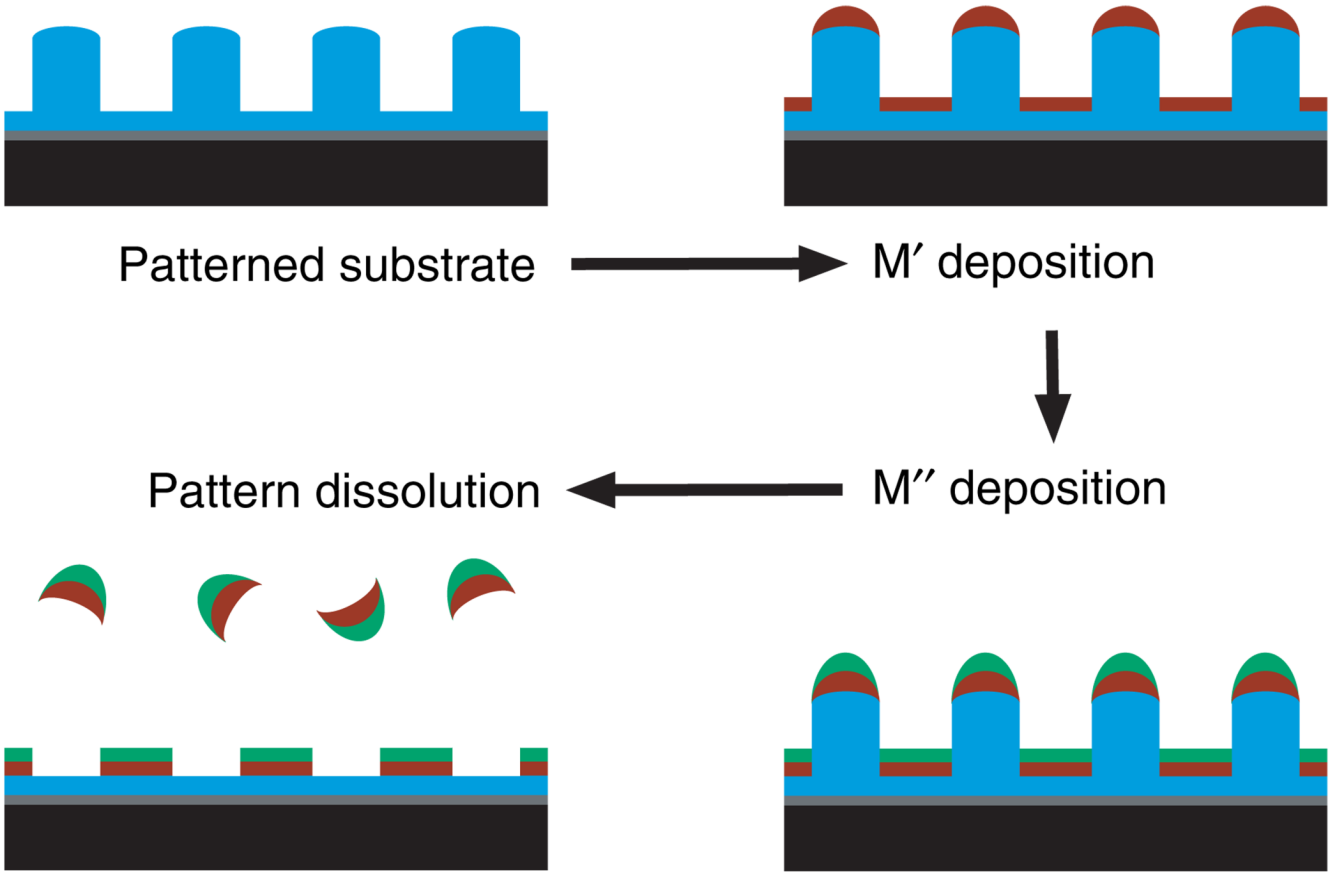

Fig. 1.
Schematic representation of the bi-metallic particle formation process.

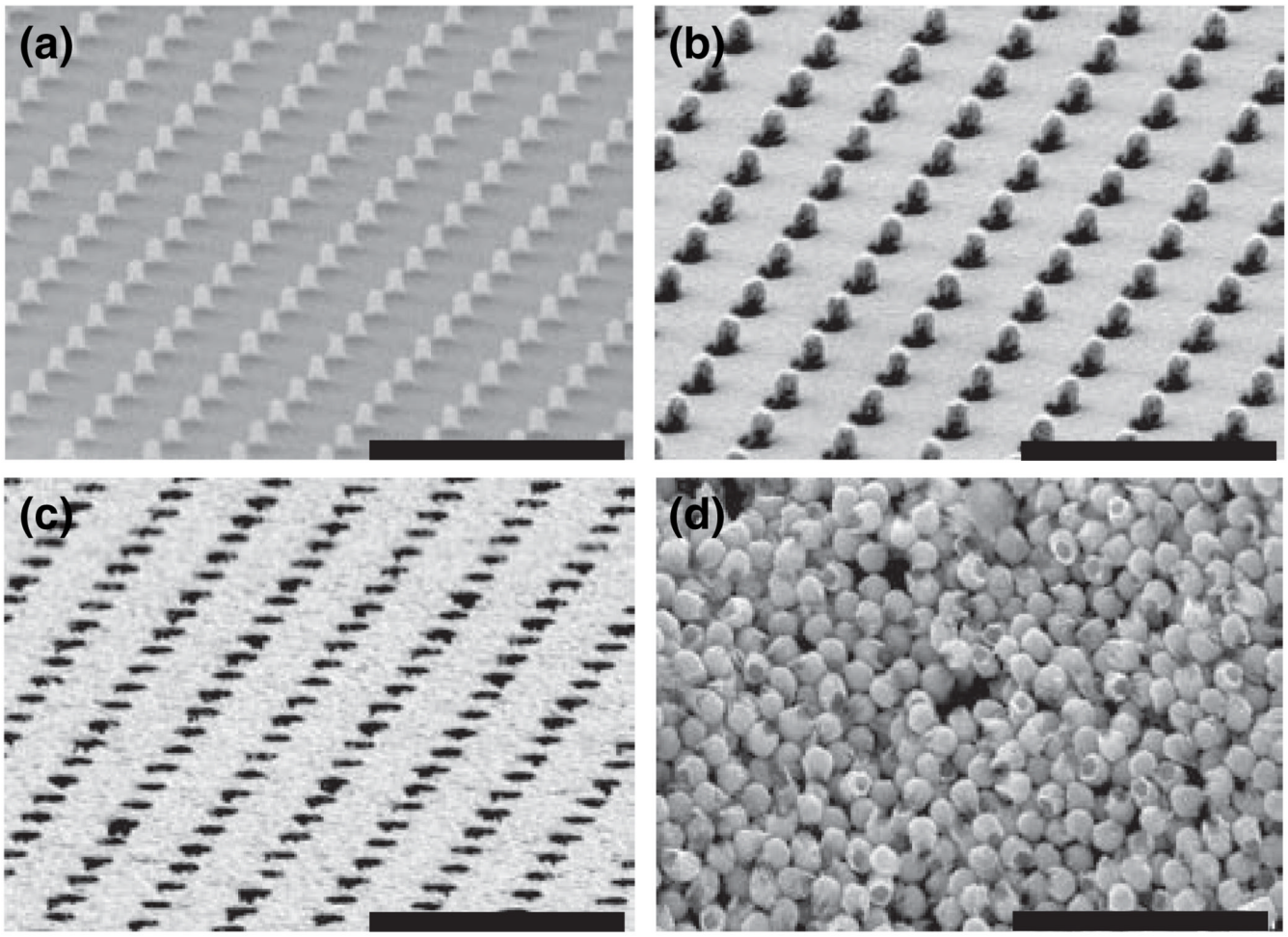

Fig. 2.
FE-SEM images detailing wafer surface through all stages of particle fabrication. (a) Lithographically defined posts; (b) metallized wafers result in a post-cap structure; (c) photoresist post dissolution is performed by soaking samples in acetone, leaving a cratered surface with particles and photoresist posts segments in acetone; (d) Au–Ni–Pd particles magnetically concentrated on a substrate. All scale bars are 2 μm.

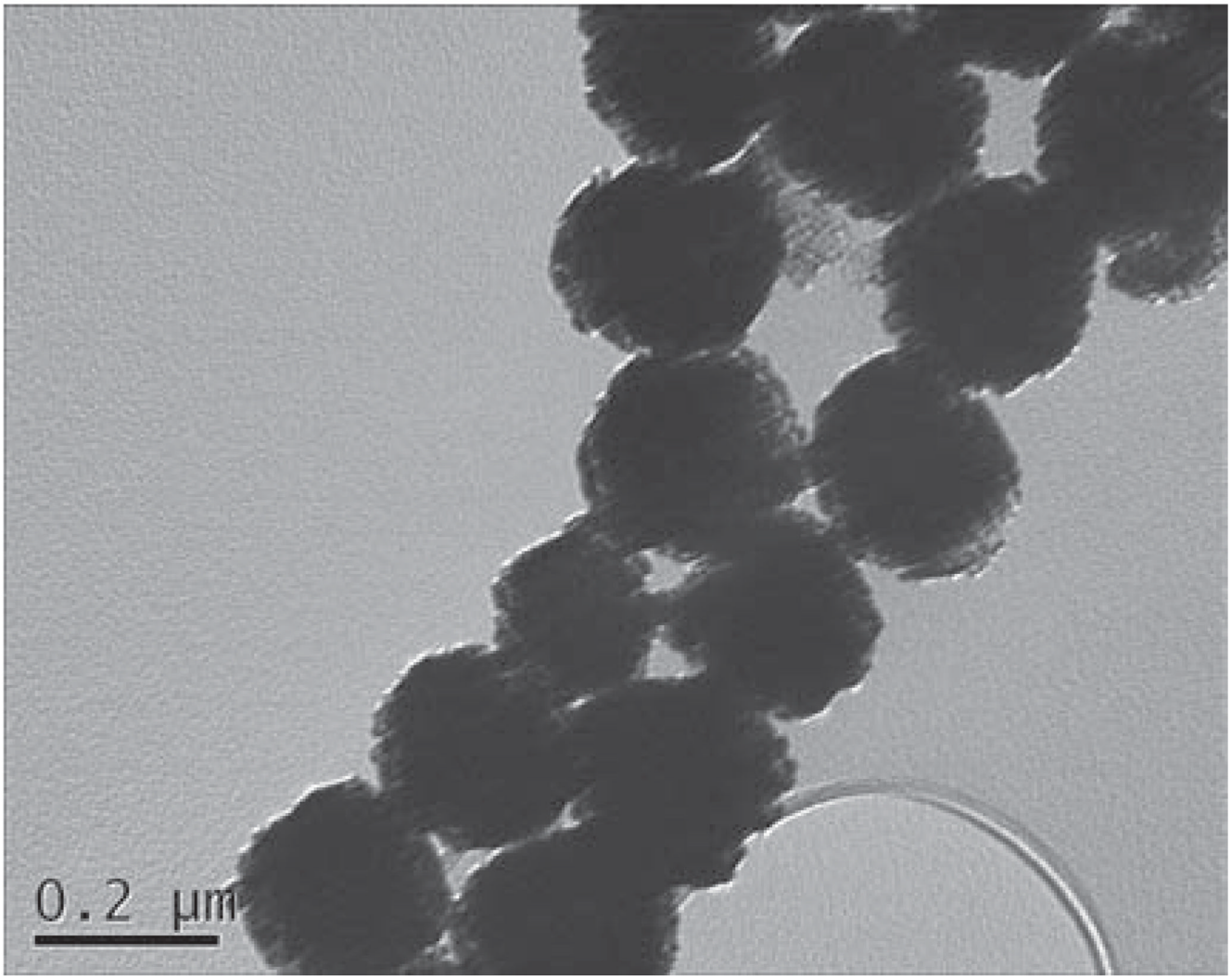

Fig. 3.
Images taken using a JEOL 2010 TEM. Images indicate spherical component of particle shape as well as size uniformity.

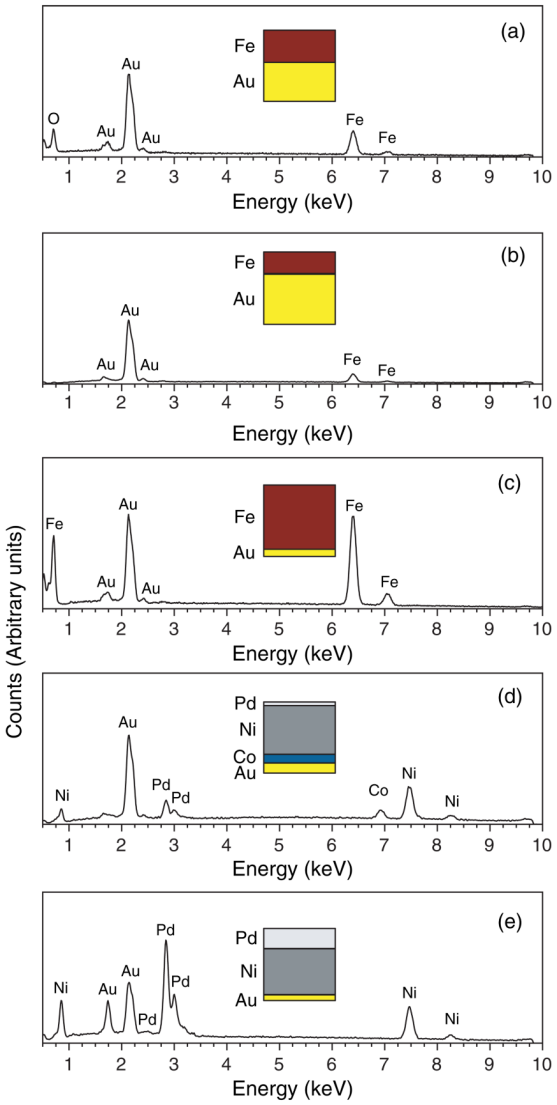

Particle ID	Au	Fe	Co	Ni	Pd
A	56.4	43.6			
B	69.2	30.8			
C	10.6	89.4			
D	13.7		12.6	68.0	5.7
E	8.2			64.1	27.7

Fig. 4.

EDS data of compositionally diverse particles. All particles were created from 99.99% pure metals (Sigma) and evaporated at 1×10^{-6} Torr from tungsten evaporation crucibles. This data represents small subset of material design possible with our post fabrication method. Inset image shows the target compositional profile of each particle type.

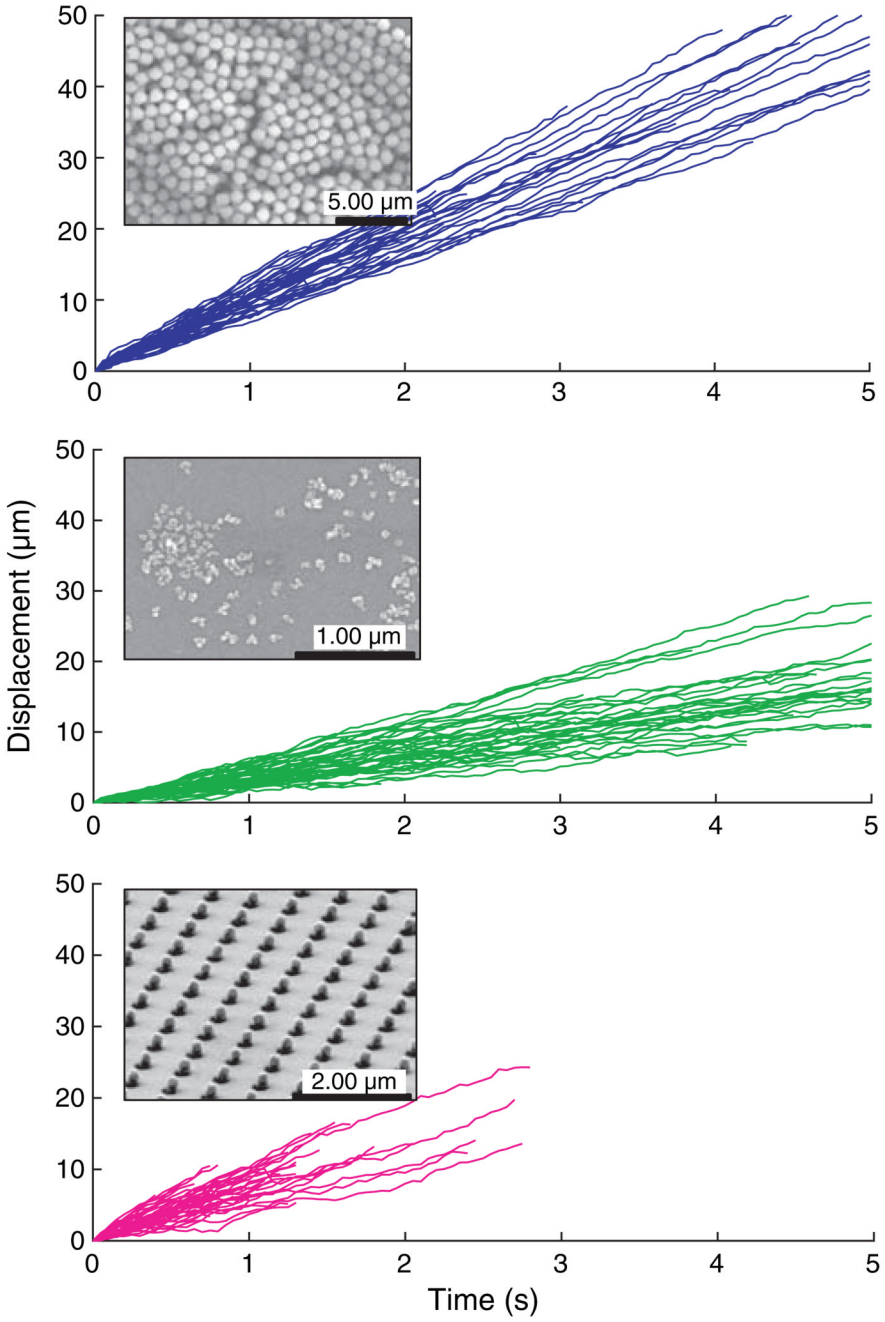

Fig. 5.

Here we show the magnet response of the particles tested. (a) Blue traces represent 1 μm Dynabeads® MyOne™ superparamagnetic beads; green traces represent Micromod 250 nm particles; purple traces represent 200 nm Fe post-particles.

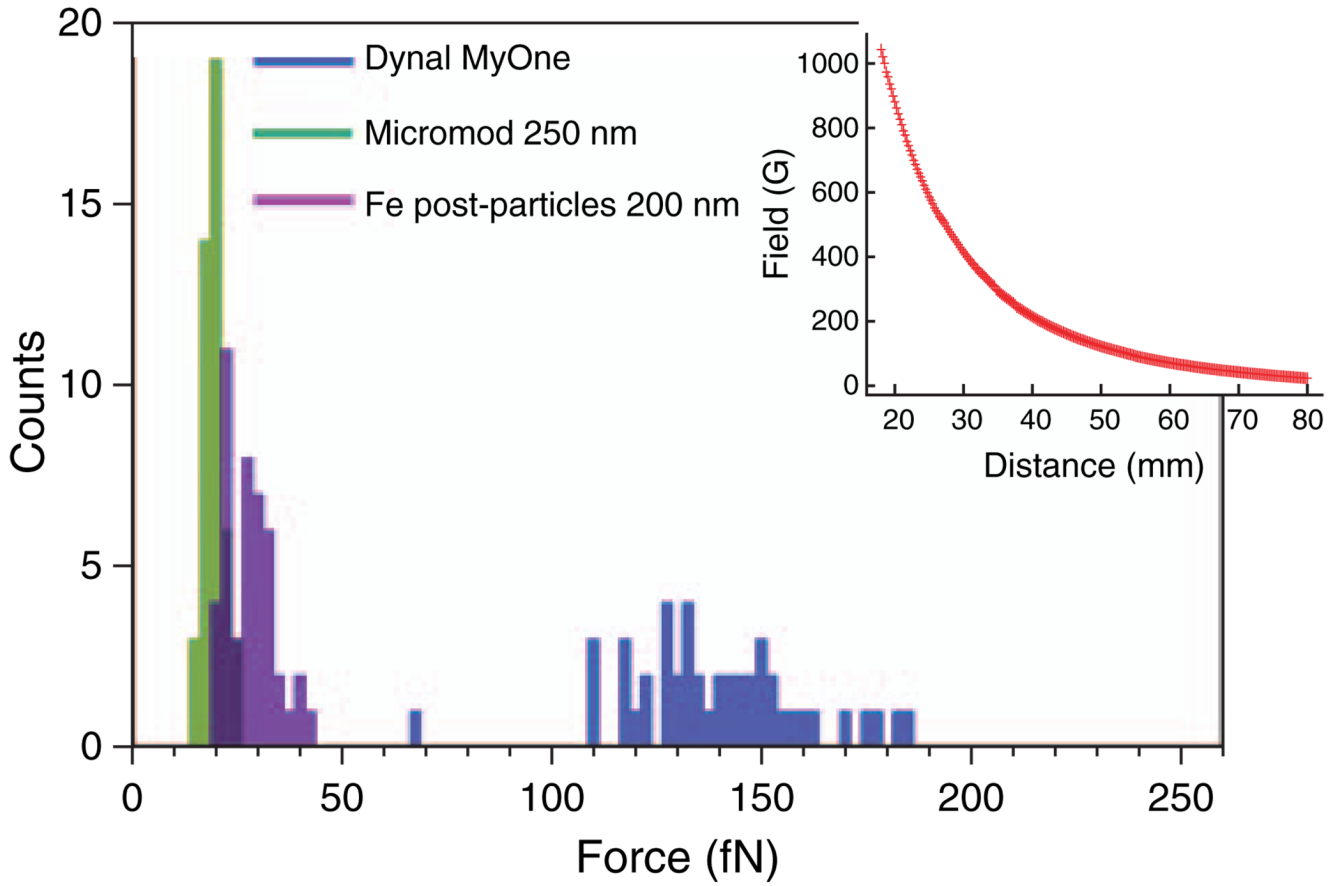

Fig. 6.

A histogram representing forces applied to particles. Force calculations are based on Stokes law and are calculated for each bead based on the tracked bead velocity. The inset represents magnetic field measurements taken at 250 μm increments measured using an F. W. Bell model 5080 gaussmeter. A Ni–Cu–Ni coated NdFeB permanent magnet (1 in. diameter, 2 in. length, K&J Magnetics) was used. A surface field of 6775 G was reported by the manufacturer.

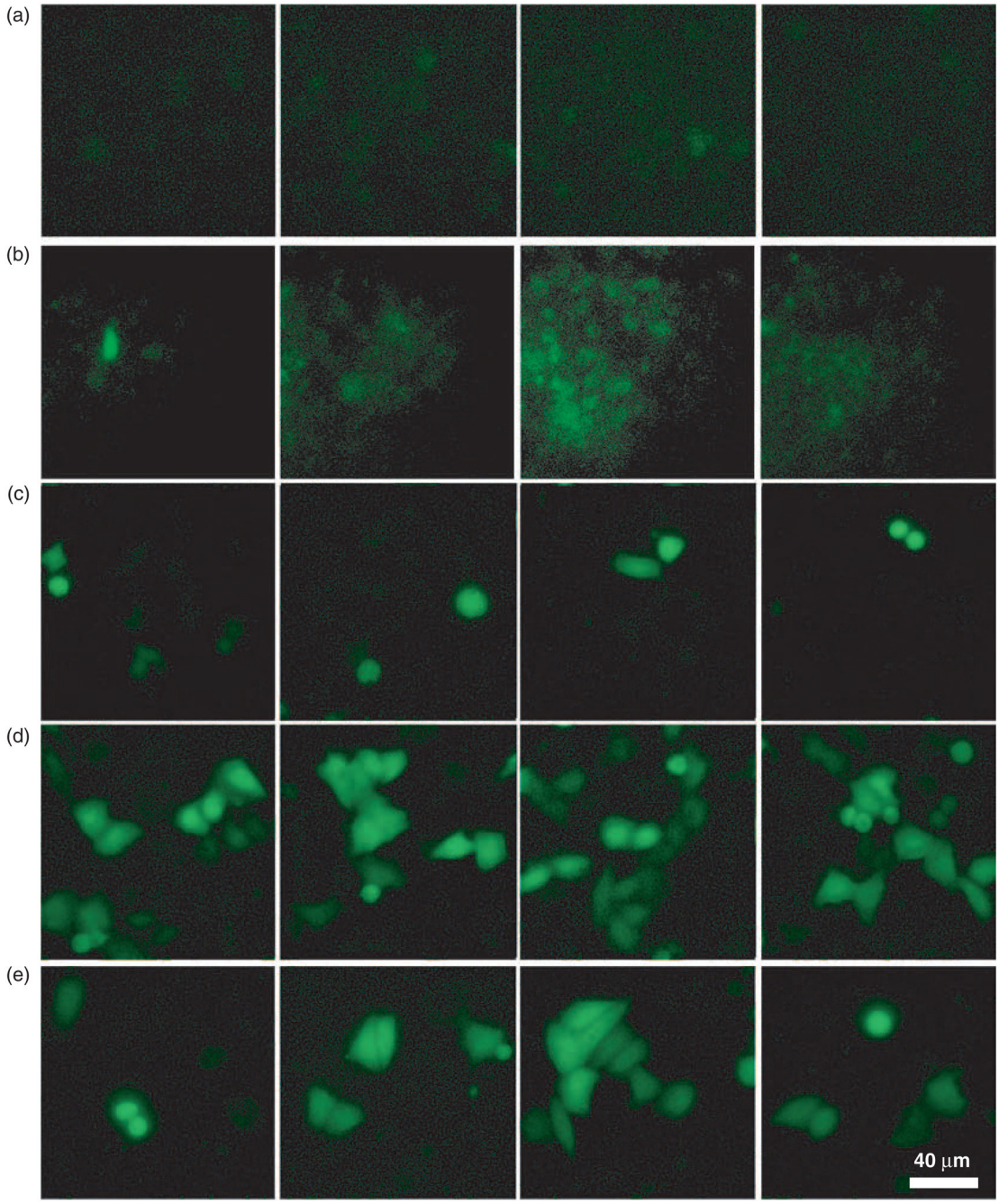

Fig. 7.
Representative images of (a) untreated cells, (b) PEI-ODN treated cells (c) particles labeled with oligonucleotide (200 nM) delivered to cells without applied magnetic field; (d) particles labeled with oligonucleotide (200 nM) delivered to cells with applied magnetic field; (e) Lipofectamine delivered to cells.

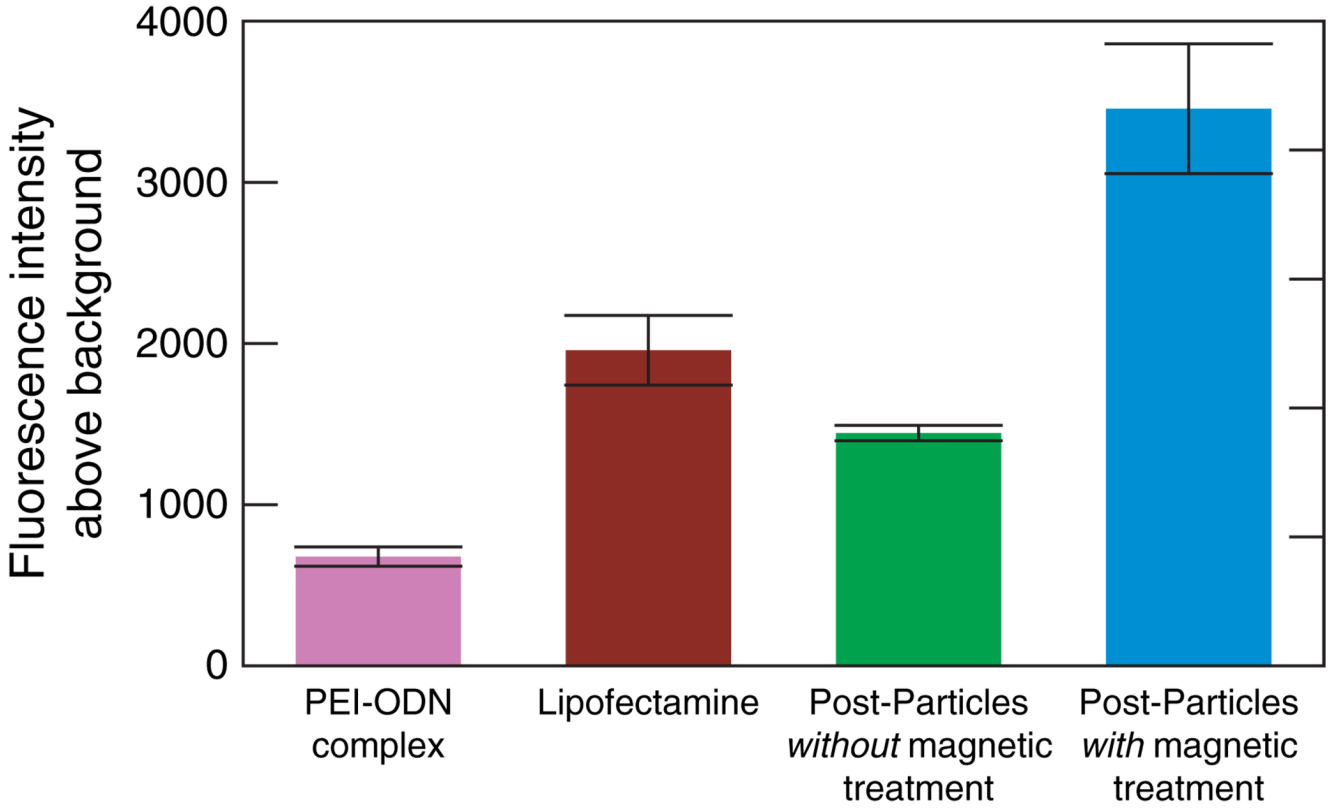

Fig. 8.
Average fluorescence intensities based on segmentation data collected across wells.

Table I

Particle	Calculated χ_v[a]	Other reports of χ_v	Calculated magnetization, M[b] ($\times 10^4$, A/m)
MyOne™	1.4	1.5[32], 1.38[33]	3.8
Micromod	12.6	6±2[34], 4.8[35]	6.0
Post-Particles	34.2	—	6.3

[a] χ_V is the volumetric susceptibility and is a measure of how magnetizable a substance can become in a given magnetic field.

[b] M is the intensity of magnetization and is defined as the quantity of magnetic moment per unit volume.